

Spatial bias in cAMP generation determines biological responses to PTH type 1 receptor activation

Alex D. White^{1,2†}, Karina A. Peña^{1†}, Lisa J. Clark^{1,3‡‡}, Christian Santa Maria⁴, Shi Liu⁵, Frédéric G. Jean-Alphonse^{1†§}, Ji Young Lee⁶, Saifei Lei^{1†||}, Zhiqiang Cheng⁴, Chia-Ling Tu⁴, Fei Fang^{1†¶}, Nicholas Szeto⁴, Thomas J. Gardella⁷, Kunhong Xiao¹, Samuel H. Gellman⁵, Ivet Bahar⁶, Ieva Sutkeviciute¹, Wenhan Chang^{4*}, Jean-Pierre Vilardaga^{1*}

Copyright © 2021
The Authors, some
rights reserved;
exclusive licensee
American Association
for the Advancement
of Science. No claim
to original U.S.
Government Works

The parathyroid hormone (PTH) type 1 receptor (PTHR) is a class B G protein-coupled receptor (GPCR) that regulates mineral ion, vitamin D, and bone homeostasis. Activation of the PTHR by PTH induces both transient cell surface and sustained endosomal cAMP production. To address whether the spatial (location) or temporal (duration) dimension of PTHR-induced cAMP encodes distinct biological outcomes, we engineered a biased PTHR ligand (PTH^{7d}) that elicits cAMP production at the plasma membrane but not at endosomes. PTH^{7d} stabilized a unique active PTHR conformation that mediated sustained cAMP signaling at the plasma membrane due to impaired β-arrestin coupling to the receptor. Experiments in cells and mice revealed that sustained cAMP production by cell surface PTHR failed to mimic the pharmacological effects of sustained endosomal cAMP production on the abundance of the rate-limiting hydroxylase catalyzing the formation of active vitamin D, as well as increases in circulating active vitamin D and Ca²⁺ and in bone formation in mice. Thus, similar amounts of cAMP generated by PTHR for similar lengths of time in different cellular locations, plasma membrane and endosomes, mediate distinct physiological responses. These results unveil subcellular signaling location as a means to achieve specificity in PTHR-mediated biological outcomes and raise the prospect of rational drug design based upon spatiotemporal manipulation of GPCR signaling.

INTRODUCTION

More than 800 individual genes encode G protein-coupled receptors (GPCRs) in humans, and their expression in various tissues is paramount for proper control of a wide range of physiological processes (1). These receptors reside predominantly at the cell surface, where they recognize and respond to an impressively diverse catalog of extracellular stimuli that range from photons and ions to small-molecule neurotransmitters and large peptide hormones (2). To explain how these receptors achieve such exquisite specificity in their biological effects, previous reports have described receptor and functional selectivity as critical determinants. Functional selectivity originally referred to empirical observations that ligands for the same GPCR can have differential propensities to activate downstream signaling pathways (referred to as biased agonism) (3, 4). In

this classical model, GPCR activation was thought to stimulate heterotrimeric G protein signaling exclusively from the cell surface in a transient manner due to subsequent recruitment of β-arrestin, which was proposed to sterically block further G protein coupling and to mediate agonist-induced receptor internalization, preventing additional rounds of stimulation by extracellular ligand. This model has been substantially revised by the discovery of several receptors that engage in sustained G protein-dependent cyclic adenosine monophosphate (cAMP) signaling from early endosomes after endocytosis (5–7). In the case of the parathyroid hormone (PTH) type 1 receptor (PTHR), PTH and a long-acting PTH analog (hereafter referred to as LA-PTH) trigger the formation of a ternary PTHR-β-arrestin-Gβγ complex that remains active after internalization and redistribution to early endosomes. This ternary PTHR complex is thought to promote and maintain a high amount of cAMP at endosomes through a series of reactions that include its reassembly with the diffusing Gαs, the conditional activation of adenylate cyclases by Gβγ, and the inhibition of cAMP-selective phosphodiesterases by activation of extracellular signal-regulated protein kinases 1 and 2 (ERK1/2) [reviewed in (7)].

Observations that the location and duration of G_s-mediated cAMP responses can be dictated in a ligand-dependent manner for a single GPCR have led to the emergence of spatiotemporal regulation in GPCR signal transduction as a previously unknown property of functional selectivity. Studies involving the PTHR have shown that full-length PTH (PTH_{1–84}, an 84-amino acid peptide) or the fully functional synthetic N-terminal fragment PTH_{1–34} and related peptide (PTH_{1–36}) stabilize distinct receptor conformations that result in cAMP responses that differ markedly in location and duration (5, 8, 9). Although all PTHR ligands stimulate transient cAMP responses from the cell surface, only PTH and PTH_{1–34} cause an additional sustained phase of cAMP generation derived from highly

¹Department of Pharmacology and Chemical Biology, School of Medicine, University of Pittsburgh, Pittsburgh, PA 15261, USA. ²Graduate Program in Molecular Pharmacology, School of Medicine, University of Pittsburgh, Pittsburgh, PA 15261, USA.

³Graduate Program in Molecular Biology and Structural Biology, School of Medicine, University of Pittsburgh, Pittsburgh, PA 15261, USA. ⁴Endocrine Research Unit, Department of Veterans Affairs Medical Center, and University of California, San Francisco, CA 94158, USA. ⁵Department of Chemistry, University of Wisconsin-Madison, Madison, WI 53706, USA. ⁶Department of Computational and Systems Biology, University of Pittsburgh School of Medicine, Pittsburgh, PA 15260, USA. ⁷Endocrine Unit, Massachusetts General Hospital and Harvard Medical School, Boston, MA 02114, USA.

*Corresponding author. Email: jpv@pitt.edu (J.-P.V.); wenhan.chang@ucsf.edu (W.C.).
†These authors contributed equally to this work.

‡Present address: Department of Biological Chemistry, University of California, Los Angeles, CA 90095, USA.

§Present address: Physiologie de la Reproduction et des Comportements (PRC), Institut National de Recherche pour l'Agriculture, l'Alimentation et l'Environnement (INRAE), Centre National de la Recherche Scientifique (CNRS), Institut Français du Cheval et de l'Equitation (IFCE), Université de Tours, 37380 Nouzilly, France.

||Present address: Center for Pharmacogenetics, University of Pittsburgh, School of Pharmacy, Pittsburgh, PA 15261, USA.

¶Present address: Department of Chemistry, Michigan State University, MI 48824, USA.

stable ligand–receptor– β -arrestin complexes that remain active in early endosomes after their internalization (5, 10–12).

These findings have subsequently been used to explain ligand-specific alterations in PTHR biological outcomes observed in vivo; however, no direct studies have been reported. For example, early studies demonstrated that injection of PTH_{1–34} and PTHrP_{1–36} into humans causes similar enhancement in the formation of new bone but discordant effects on ionized serum Ca^{2+} (sCa^{2+}) and vitamin D amounts, with lesser effects observed for PTHrP_{1–36} (13). In addition, the PTHrP analog abaloparatide, which triggers transient cAMP production confined to the cell surface, has been shown to efficiently promote bone formation with a reduced hypercalcemic effect when compared to PTH_{1–34}. Both PTH_{1–34} and abaloparatide are U.S. Food and Drug Administration approved for the treatment of osteoporosis. Despite these advancements, whether the spatial versus the temporal dimension of cAMP signaling encodes ligand-dependent PTHR biological specificity remains unknown.

Here, we addressed this question by developing a location-biased PTHR peptide ligand through amino acid epimerization at position 7 of PTH_{1–34} (referred to as PTH^{7d}). We demonstrated that this ligand stabilized a receptor conformation that failed to recruit β -arrestins and stimulated sustained cAMP exclusively from the cell surface, thus indicating that spatial bias of cAMP generation can be triggered by single amino acid epimerization of the ligand peptide. Subsequent studies in mice and polarized human epithelial kidney cells comparing the actions of PTH^{7d} and an LA-PTH analog (14) that potently promotes endosomal cAMP production revealed that homeostatic control of sCa^{2+} and active vitamin D concentrations specifically requires sustained cAMP generation from endosomal compartments as opposed to sustained cAMP production from the plasma membrane. This study highlights the potential for delineating spatial and temporal signaling bias in rational drug design and the development of therapeutics with enhanced biological specificity.

RESULTS

Selection and characterization of a location-biased PTH analog

We have previously shown that translocation of PTH-PTHR signaling complexes from the cell surface to early endosomes is β -arrestin-dependent (10, 11). We reasoned that a PTHR ligand that stimulates cAMP production but fails to recruit β -arrestin would cause a shift in sustained cAMP generation from endosomes to the cell surface, thus permitting determination as to how the cellular localization of signaling responses influences PTHR biology.

To help design a PTH analog with the desired bias and to better understand the bioactive domains and key functional determinants in PTH, we analyzed an anisotropic network model (ANM) of PTH-bound receptor that we previously reported (15). Briefly, the ANM probes the collective motion of the PTH-PTHR complex based on the position of Ca atoms and thus unveils cooperative structural changes upon ligand binding (16). Here, we focused on one mode of motion that displayed the opening and closing of the receptor intracellular face, reflecting a motion that occurs during receptor activation. To determine which PTH residues would elicit cooperative responses consistent with PTHR activation, we examined the cross-correlations between all PTH residues with Thr³⁹² of the receptor, which is located near the third intracellular loop (ICL3), a region where conformational rearrangements associated

with receptor activation (fig. S1A). PTH residues 1 to 10 had strong positive (>0.5) cross-correlations with the intracellular part of the receptor, which supports previous observations that this region constitutes the signaling portion of the peptide (17, 18). Our ANM analysis suggested that the opening and closing of the intracellular region is allosterically coupled to the structural changes at residues interacting with the N-terminal portion of PTH that includes residues 1 to 10 (fig. S1A). From our previous investigations, we discerned that PTH residues 1 to 4 are specifically determinant to switch “on” the receptor active state (12, 14, 19). We decided to focus on PTH residues 5 to 7, 9, and 10, which exhibited high cross-correlation values (>0.6), and thus, we hypothesized that their substitutions in PTH_{1–34} (hereafter referred to as PTH^{WT}) may bias receptor coupling to G proteins instead of β -arrestin and thus favor signaling at the plasma membrane instead of at endosomes. We aimed to introduce a minimal chemical modification of the interrogated residue; therefore, we chose the epimerization (L- to D-amino acid residue) instead of conventional alanine scanning substitution. The assumption that amino acids 5 to 10 of PTH^{WT} determine signaling bias was tested by comparing time courses of cAMP production and β -arrestin 2 (β -arr2) recruitment to PTHR. PTH^{WT} and some of its diastereomers (PTH^{7d} and PTH^{10d}) stimulated indistinguishable increases in cAMP (fig. S1B), but only PTH^{WT} and PTH^{10d} stimulated the interaction of PTHR with β -arr2 (fig. S1C).

We further examined the signaling properties of PTH^{7d} in human embryonic kidney (HEK293) cells stably expressing recombinant human PTHR. This modification did not alter the binding affinity in equilibrium competition assays in intact cells (fig. S2) nor did it cause changes in the potency [median effective concentration (EC₅₀)] or maximal efficacy (E_{\max}) of cAMP production in luciferase-based accumulation assays (Fig. 1A and Table 1). In contrast, PTH^{7d} displayed markedly impaired recruitment of β -arrestin compared to PTH^{WT} or LA-PTH (a long-acting chimeric PTH/PTHrP peptide whose N- and C-terminal fragments correspond to PTH_{1–15} and PTHrP_{16–34}, respectively), as measured by bioluminescence resonance energy transfer (BRET) in cells stably expressing luciferase-tagged PTHR (PTHR^{RLuc8}) and Venus-tagged β -arr1 or β -arr2 (Fig. 1B). This effect was confirmed by both Förster resonance energy transfer (FRET)-based time courses in cells transiently coexpressing PTHR fused to cyan fluorescent protein (PTHR^{CFP}) and β -arr2 fused to yellow fluorescent protein (β -arr2^{YFP}) (Fig. 1C), in coimmunoprecipitation assays (Fig. 1D), and in photocrosslinking experiments (fig. S3).

We next sought to determine the time course of cAMP generation for PTH^{7d} using the FRET-based sensor Epac^{CFP/YFP}. Recordings in single cells revealed that PTH^{7d} induced sustained cAMP responses upon ligand washout that were highly similar in magnitude and duration to those induced by PTH^{WT} and LA-PTH (Fig. 2A). Despite similar cAMP response kinetics, we subsequently determined that prolonged cAMP generation observed for PTH^{7d} was derived from ligand-receptor complexes retained at the cell surface, because inclusion of a cell-impermeable PTHR antagonist (D-Trp¹², Tyr³⁴-bPTH_{7–34}) (20) in the washout buffer completely abolished the sustained phase of PTH^{7d}-mediated cAMP generation but had moderate or no effect in analogous experiments using PTH^{WT} or LA-PTH, respectively (Fig. 2B). Consistent with this finding, blockade of receptor internalization by expression of a dominant-negative dynamin mutant (DynK44A) significantly reduced cAMP responses induced by PTH^{WT}, whereas those for PTH^{7d} were unaffected (fig. S4).

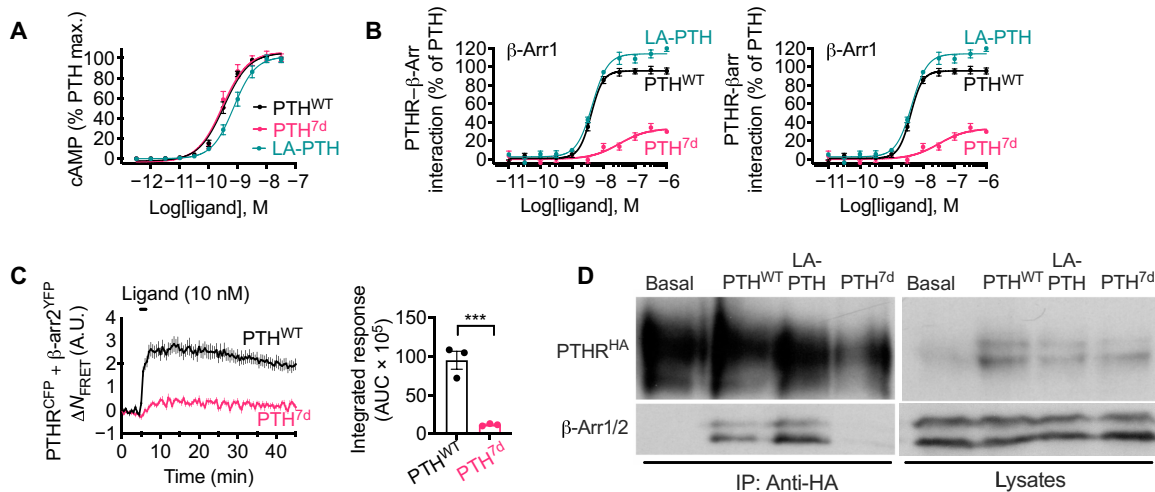


Fig. 1. Characterization of a G_s-biased PTH analog generated by amino acid isomerization. (A and B) Concentration-response curves for PTH^{WT}, LA-PTH, and PTH^{7d} in cAMP accumulation (A) or in β-arr1 or β-arr2 recruitment (B) assays. Data are means ± SEM from $N = 5$ independent experiments. (C) Time course and integrated response of β-arr2 recruitment measured by FRET in HEK293 cells transiently expressing PTHR^{CFP} and β-arr2^{YFP} after brief stimulation with 10 nM PTH^{WT} or PTH^{7d}. Data are means ± SEM from $N = 3$ independent experiments with $n = 28$ to 33 cells per experiment. *** $P < 0.005$ by *t* test. A.U., arbitrary units. (D) Recruitment of endogenous β-arr1 and β-arr2 (β-arr1/2) to PTHR detected by coimmunoprecipitation with HA-tagged PTHR (HA-PTH) stably expressed in HEK293 cells. Cells were challenged with 100 nM of either PTH^{WT}, LA-PTH, or PTH^{7d}. Blot is representative of two independent experiments.

Table 1. Binding isotherm and signaling properties. Binding in intact cells was performed with tetramethylrhodamine-labeled PTH (PTH₁₋₃₄), and the binding affinity constant K_b was calculated after the Cheng and Prusoff correction. For R⁰ and R^G, the binding was performed in plasma membrane extracts from HEK293 cells lacking G_s by CRISPR-Cas9 deletion and transiently transfected with PTHR without (R⁰) or with (R^G) G_s-ND. Data are means ± SEM from $N = 3$ (binding), $N = 4$ (cAMP), and $N = 5$ (β-arr1 and β-arr2) independent experiments. pEC₅₀ = $-\log_{10}(EC_{50})$.

Ligands	Binding		Binding		Binding	
	Intact cells		R ⁰		R ^G	
	K_b (nM)	P	IC ₅₀ (nM)	P	IC ₅₀ (nM)	P
PTH ^{WT}	4.97 ± 0.92	1.00	4.70 ± 1.33	1.00	0.10 ± 0.04	1.00
PTH ^{7d}	4.27 ± 0.80	1.00	17.14 ± 3.28	0.015	0.10 ± 0.04	1.00
Ligands						
	cAMP		β-arr1		β-arr2	
	pEC ₅₀	E_{max}	pEC ₅₀	E_{max}	pEC ₅₀	E_{max}
PTH ^{WT}	9.36 ± 0.04	100	8.32 ± 0.04	100	8.37 ± 0.05	100
PTH ^{7d}	9.45 ± 0.08	99 ± 5	7.76 ± 0.08	40 ± 2	7.71 ± 0.11	37 ± 3

Furthermore, real-time analysis of receptor trafficking in cells stably expressing PTHR N-terminally tagged with superecliptic (SEP) pHluorin, a pH-sensitive green fluorescent protein (GFP) variant that exhibits fluorescence intensity reduction in acidic environments (21), showed only modest internalization upon PTH^{7d} stimulation when compared to PTH^{WT} and LA-PTH (Fig. 2C).

Last, we previously reported that the endosomal cAMP pool diffuses more effectively into the nucleus than does the plasma membrane-adjacent pool and thus represents a rate-limiting step for nuclear cAMP-mediated protein kinase A (PKA) activation (22, 23). We verified that here by comparing nuclear cAMP accumulation and PKA activity over time in response to LA-PTH compared with PTH^{7d} (Fig. 2D). Collectively, our signaling characterization data indicate that amino acid epimerization at position 7 of PTH results in a location and G_s-biased peptide ligand that differs from PTH^{WT}

and LA-PTH solely by the cellular localization of active signaling complexes involved in sustained cAMP responses. Specifically, PTH^{7d} stimulates G protein-dependent production of cAMP at the plasma membrane but does not stimulate β-arrestin-dependent internalization of PTHR and subsequent generation of cAMP at endosomes. We subsequently examined the molecular basis for these signaling discrepancies, as well as their consequences *in vivo*.

Molecular basis for impaired PTH^{7d} function

Given the well-established importance of β-arrestin coupling to the PTHR in permitting sustained cAMP generation at endosomes in response to PTH^{WT}, we sought to investigate the molecular mechanisms that underlie the relative inability of PTH^{7d} to promote this interaction, as well as its consequences for both cell biological and pharmacological processes. Recruitment of β-arrestin to activated

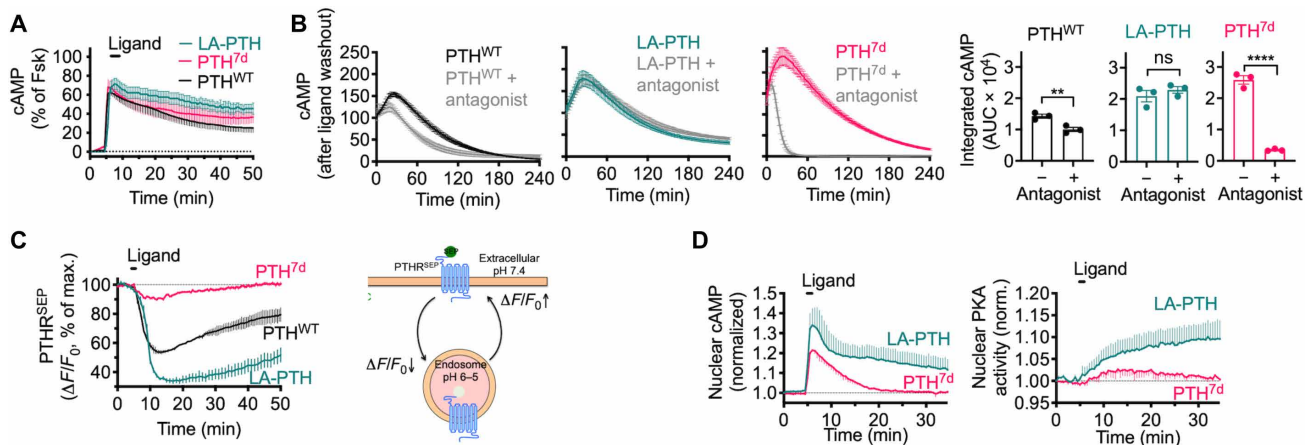


Fig. 2. Location bias of PTH^{7d} signaling. (A) Averaged cAMP time course responses after brief stimulation with 10 nM PTH^{WT}, LA-PTH, or PTH^{7d}. Percentage of cAMP responses is relative to the response in the presence of forskolin (Fsk). Data are means \pm SEM from $N = 3$ independent experiments with $n = 20$ to 26 cells per experiment. (B) Time courses and integrated responses after washout of 1 nM PTH^{WT}, PTH^{7d}, or LA-PTH in the presence or absence of cell-impermeable antagonist. Data are means \pm SEM from $N = 3$ experiments. $P = 0.01$ (PTH^{WT}), $P = 0.39$ (LA-PTH), and $P < 0.0001$ (PTH^{7d}) by t test. ** $P < 0.01$, *** $P < 0.0001$. ns, not significant. (C) Time courses of internalization and recycling of PTHR tagged with superecliptic pHluorin (PTHR^{SEP}) in response to 100 nM ligand measured by time-lapse confocal microscopy. A schematic depicting the measured values is also shown. Data are means \pm SEM from $N = 3$ experiments with $n = 11$ to 14 cells per experiment. (D) Averaged nuclear cAMP and PKA activity time course experiments after brief stimulation with 30 nM PTH^{7d} or LA-PTH. Data are means \pm SEM from $N = 3$ independent experiments with $n = 9$ to 14 cells per experiment.

GPCRs is thought to occur after phosphorylation of serine and threonine residues within intracellular receptor domains, specifically the ICL3 and C-terminal tail, by GPCR kinases. Furthermore, it has been proposed that receptor phosphorylation status serves as the foremost determinant for GPCR- β -arrestin interactions, a paradigm commonly referred to as the phosphorylation barcode hypothesis (24–26). Accordingly, we examined whether PTH^{WT} and PTH^{7d} triggered distinct phosphorylation patterns in the PTHR that differentially permitted distinct interactions with β -arrestins by performing stable isotope labeling by amino acids in cell culture (SILAC)-based quantitative proteomics (fig. S5A). By liquid chromatography with tandem mass spectrometry (LC-MS/MS), we identified 10 phosphorylation sites located in the C-terminal tail and ICL3 in response to 5 min of PTH^{WT} or PTH^{7d} stimulation at a concentration of 30 nM (fig. S5B and fig. S6, A and B). Although β -arrestin recruitment is usually considered to be driven by the phosphorylation status of a GPCR (27), we found no significant differences in the sites or extent of phosphorylation between PTH^{WT} and PTH^{7d} treatments. In an effort to confirm our hypothesis that β -arrestin recruitment to hormone-activated PTHR may occur independently of receptor phosphorylation, we assessed the extent of PTH^{WT}-triggered β -arrestin recruitment to phosphorylation-deficient PTHR mutants, where identified phosphorylated serine and threonine residues in either ICL3 (PTHR^{PD-ICL3}) or the C-terminal tail (PTHR^{PD-Ct}) were mutated to alanine. Our immunoprecipitation analysis revealed that whereas the absence of phosphorylation sites in the receptor's C terminus had no effect on β -arrestin recruitment, the elimination of phosphorylation sites within ICL3 severely impaired β -arrestin recruitment to PTHR (fig. S7A). Taking into account the lack of quantitative LC/MS-MS data on ICL3 phosphorylation status, this observation suggests that ICL3 might be a determinant of initial β -arrestin recruitment to PTHR, whereas the C terminus itself contributes to the stabilization of β -arrestin–receptor complexes as previously proposed (28). The latter hypothesis was supported by FRET time course experiments using the PTHR^{PD-Ct} mutant, which showed

that receptor phosphorylation did not contribute to the initial coupling of the PTHR to β -arr2 (fig. S7B) but rather to the stability of the complex over time (fig. S7C), a result consistent with earlier work (28). Overall, this finding suggests that alteration in β -arrestin recruitment observed for PTH^{WT} and PTH^{7d} was not caused by defective receptor phosphorylation at the C terminus, but altered phosphorylation of ICL3 or conformational changes because of alanine substitutions might be the cause of diminished β -arrestin recruitment to PTH^{7d}-bound PTHR.

Because the ICL3 is an immediate indicator of GPCR activation status, we considered that these ligands may uniquely stabilize distinct active PTHR conformations. This hypothesis was investigated experimentally by comparing the capacity of ligands to stabilize the G protein-coupled (R^G) and G protein–uncoupled (R^0) conformations of PTHR using binding isotherms measured in cell membrane extracts. Compatible with the indistinguishable binding affinity of PTH^{WT} and PTH^{7d} for the receptor in intact cells, these ligands displayed identical affinities for the R^G conformation in vitro (Fig. 3A). In contrast, PTH^{7d} had decreased binding affinity for the R^0 conformation (Fig. 3A and Table 1), which is usually associated with sustained cAMP originating from endosomes (29), suggesting that PTH^{7d} stabilizes a distinct receptor conformation. We further confirmed that PTH^{WT} and PTH^{7d} stabilized distinct signaling PTHR conformations using PTHR^{CFP/YFP}, an intramolecular FRET-based PTHR sensor (scheme in Fig. 3B) that reports conformational rearrangements as the receptor switches from inactive to active states in response to ligand binding (30). Perfusion of PTH^{WT} to cells expressing this sensor induced a fast increase in the FRET ratio F_{YFP}/F_{CFP} with a time constant $\tau \approx 3.4$ s (Fig. 3C). In contrast, perfusion of PTH^{7d} induced a FRET change of similar kinetics but substantially lower magnitude than that by PTH^{WT}. Because FRET depends on the distance and the dipole-dipole orientations of fluorophores, these results imply that PTH^{7d} stabilizes a PTHR conformation distinct from that seen in response to PTH^{WT}.

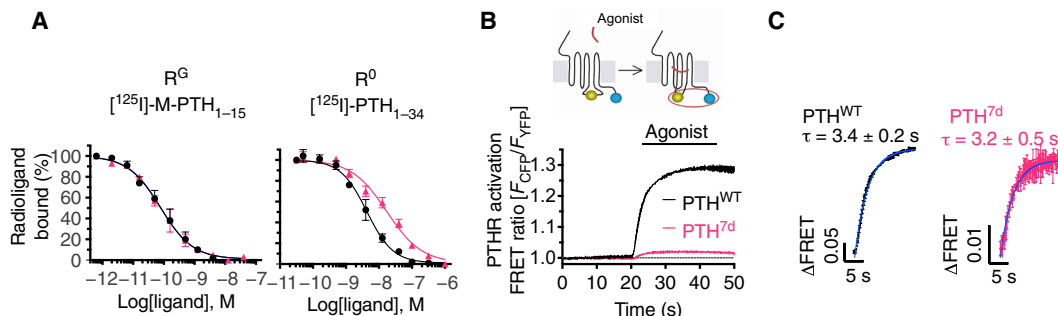


Fig. 3. Molecular changes induced by PTH^{7d}. (A) Competition binding at equilibrium with ^{125}I -PTH₁₋₁₅ and ^{125}I -PTH₁₋₃₄ as radioligands to detect the R^G and R^0 states of PTHR, respectively. Data are means \pm SEM from $N = 5$ independent experiments with duplicate wells for each concentration. (B and C) The inset shows a schematic of the FRET-based PTHR activation sensor (PTHR^{CFP/YFP}) with YFP (yellow) fused to ICL3 and CFP (blue) attached to the receptor C-terminal tail. The graph shows averaged time courses of PTHR activation by recording changes of the FRET ratio in HEK293 cells expressing PTHR^{CFP/YFP} with the initial value at $t = 0$ set to 1 (B) and kinetics of PTHR activation (C). Cells were continuously perfused with control buffer or 1 μM agonist (horizontal bar). Data are means \pm SD from $N = 2$ independent experiments. Note that the FRET data are expressed as $F_{\text{CFP}}/F_{\text{YFP}}$, resulting in a positive change upon agonist stimulation.

These observations were further supported by molecular dynamics (MD) simulations. We used the recently reported 3.0- \AA cryo-electron microscopy (cryo-EM) structure of active-state PTHR bound to G_s and LA-PTH [Protein Data Bank (PDB) 6NBF] (14) to generate initial models of PTH^{WT}- and PTH^{7d}-bound PTHR for triplicate 200-ns MD simulations. In the initial PTH^{7d}-PTHR model, D-Leu⁷ is unfavorably close to neighboring receptor transmembrane helix 7 (TM7) residues Trp⁴³⁷ [corresponding to position 7.35 in the Wootten numbering scheme for class B GPCRs (31)] and Met⁴⁴¹ (7.39 in the Wootten scheme) (fig. S8A), and simulations revealed that the D-Leu⁷ side chain shifts to mirror L-Leu⁷ nonpolar interactions in the PTH^{WT}-PTHR model (fig. S7B). We found that this shift induces a kink in the N-terminal portion of PTH^{7d} helix toward TM6 (fig. S8B), which subsequently permits additional polar interactions between Glu⁴ of PTH^{7d} and PTHR residues that are not observed for PTH^{WT} (fig. S8, C and D, and table S1). In the active-state cryo-EM structure of PTHR, Glu⁴ promotes an extensive polar interaction network that stabilizes the outward kink of TM6, which is considered a prerequisite for coupling to G proteins (12, 14). The increased polar contacts by Glu⁴ of PTH^{7d} further extends this polar interaction network relative to the PTH^{WT}-bound receptor, resulting in a more pronounced TM6 kink and a slight shift of the N-terminal portion of TM6 induced by PTH^{7d} (fig. S8, E and F). Although speculative, these MD predictions are consistent with FRET assays, indicating different PTHR conformations stabilized by PTH and PTH^{7d}.

Differential pharmacological actions of PTH^{7d}, PTH^{WT}, and LA-PTH in mice

The PTHR is the main regulator of bone remodeling and serum mineral ion (inorganic phosphate and Ca^{2+}) homeostasis (17). Despite previous reports demonstrating ligand-dependent modulation of these physiological processes, whether the location or the duration of the cAMP response is determinant remains unclear. We thus compared the effects of PTH^{7d}, PTH^{WT}, and LA-PTH on these parameters in mice after 4 weeks of daily injection (40 $\mu\text{g}/\text{kg}$ body weight). Examination of skeletal parameters by microcomputed tomography (Fig. 4A) further highlighted the physiological significance of spatial organization in PTHR-mediated signaling. Whereas all three ligands caused a moderate but significant increase in total bone volume (TV) of the metaphysis at the distal femur (Fig. 4B),

only PTH^{WT} and LA-PTH led to a significant increase in trabecular (Tb) bone fractions [Tb bone volume relative to TV (Tb.BV/TV)] and thickness (Tb.Th) when compared to vehicle control (Fig. 4B). Despite its ability to prolong the cAMP response at the cell membrane, PTH^{7d} induced a trend of increase in Tb.BV/TV that is comparable to the skeletal response to PTH^{WT}. In addition, LA-PTH treatment resulted in an increase in Tb number (Tb.N) that was markedly distinct from that observed for PTH^{WT} and PTH^{7d} (Fig. 4B). These data suggest that endosomal cAMP has a greater impact on skeletal homeostasis than does plasma membrane-associated cAMP.

Analysis of the effects on mineral ion homeostasis revealed that each ligand caused similar reductions in serum phosphate ion (sPi) amounts (Fig. 4C), consistent with the previously reported inhibition of phosphate uptake by PKA-dependent phosphorylation of NHERF1 (Na^+/H^+ exchanger regulatory factor-1) in the cytoplasm (32). However, acute increases in sCa²⁺ occurred only in response to PTH^{WT} and LA-PTH, but not PTH^{7d}, compared to vehicle control (Fig. 4C). Given that blood samples were taken 2 hours after the last injection of peptide, the acute actions of the peptide on Ca²⁺ and Pi were likely due to the responses in the kidney, instead of the bone. Previous studies have established that PTHR ligands may indirectly influence these processes by increasing 1,25-dihydroxy vitamin D (1,25D), the active form of vitamin D, in renal cells (33). Consistent with calcemic responses was the acute or sustained increase in circulating 1,25D upon injection of PTH^{WT} or LA-PTH, respectively, into mice that was completely absent in mice treated with PTH^{7d} (Fig. 4D and fig. S9, A to D). Pharmacokinetic analysis of serum from mice treated with LA-PTH or PTH^{7d} confirmed that in vivo effects were not influenced by differential degradation of these peptides (fig. S10). The impaired action of PTH^{7d} compared to PTH^{WT} and LA-PTH as it relates to increase in 1,25D may arise from deficient induction of the 25-hydroxyvitamin D 1- α hydroxylase (referred to as 1- α [OH]ase), the rate-limiting enzyme that catalyzes the conversion of 25-hydroxyvitamin D in renal proximal tubule epithelial cells. This premise was supported by the observation that basolateral stimulation with LA-PTH and PTH, but not PTH^{7d}, caused a significant increase in the production of 1- α [OH] ase in polarized Madin-Darby canine kidney (MDCK) cells (Fig. 5, A and B), despite the ability of both ligands to induce

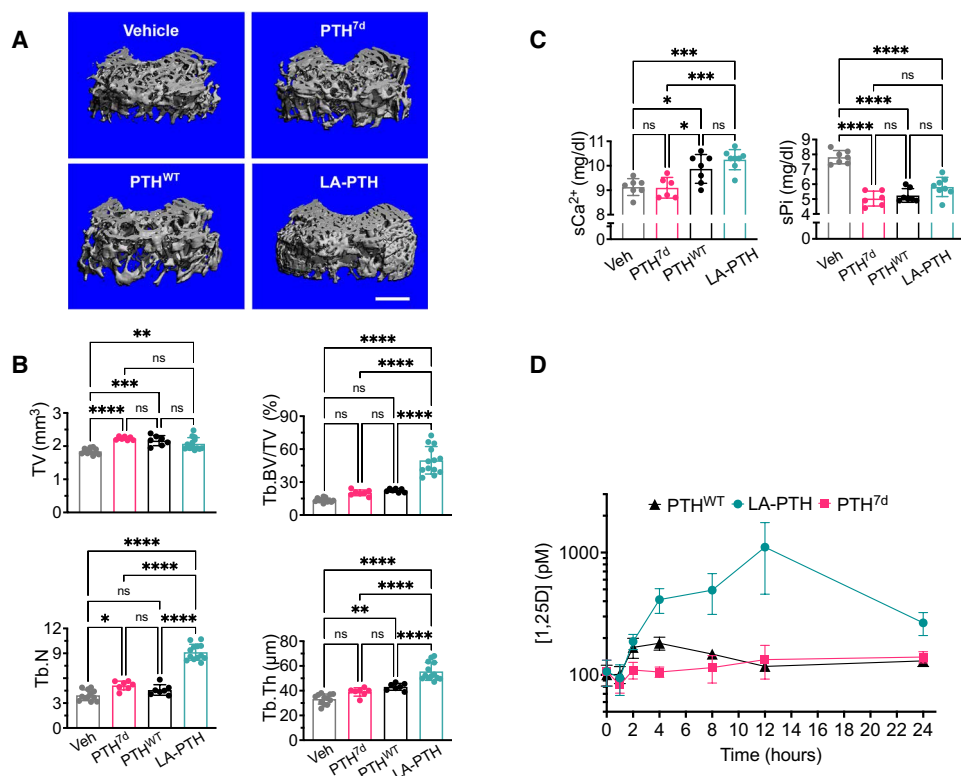


Fig. 4. Differential pharmacological actions of PTH^{7d}, PTH^{WT}, and LA-PTH in mice. (A) Three-dimensional (3D) reconstructed microcomputed tomography (μCT) images of secondary spongia at the distal femurs of mice treated with vehicle, PTH^{7d}, PTH^{WT} (PTH¹⁻³⁴), or LA-PTH. Scale bar, 500 μm. (B) Quantifications of skeletal parameters in trabecular (Tb) bone of distal femur, including total bone volume (TV), ratio of Tb bone volume (Tb.BV) to TV (Tb.BV/TV), Tb number (Tb.N), and Tb thickness (Tb.Th). Parameters were assessed in mice subjected to daily injections of PTH^{7d}, PTH^{WT}, LA-PTH, or vehicle (Veh) for 4 weeks. Data are means ± SD from N = 7 mice per group for PTH^{7d} and PTH^{WT} injections and N = 14 mice per group for LA-PTH and Veh injections. *P < 0.03, **P < 0.0005, and ****P < 0.0001 versus Veh control mice by one-way ANOVA with Tukey-Kramer post hoc test. (C) Quantification of sCa²⁺ and phosphate (sPi) measured 2 hours after the last of the 4-week daily injections of PTH^{7d}, PTH^{WT}, LA-PTH (40 μg/kg body weight per injection), or Veh. Data are means ± SD from N = 7 mice per group. *P < 0.03, **P < 0.002, ***P < 0.0002, and ****P < 0.0001 versus Veh control mice by one-way ANOVA with Tukey-Kramer post hoc test. (D) Quantification of serum 1,25D measured in mice before or 1, 2, 4, 8, 12, or 24 hours after a single injection of PTH, PTH^{7d}, or LA-PTH. Data are means ± SD from N = 7 mice per time point per drug and 15 mice for time "0" controls. Statistical analysis is shown in the Supplementary Materials (fig. S9).

similar cytosolic cAMP responses in this cell line, and with the PTH^{7d} response being restricted to the basolateral membrane (Fig. 5, C and D). Together, these findings provide evidence that the location of sustained cAMP signaling serves as a critical regulator for PTHR-mediated effects on sCa²⁺, with increases in 1-α[OH]ase and activation of vitamin D as clear underlying determinants.

DISCUSSION

The present work identifies that amino acid epimerization at a single position in a class B GPCR peptide ligand may provide a means to exquisitely probe ligand-dependent signaling determinants and pharmacological consequences without significantly altering ligand binding affinity or stability in vivo. In the case of PTH^{7d}, L-to-D isomerization at position 7 of PTH revealed significant modulation of PTHR-β-arrestin interactions and thus a shift in the cellular localization of sustained cAMP signaling from endosomes to the plasma membrane. Such negative modulation of PTHR-β-arrestin

interaction by PTH^{7d} is likely a result of a distinct receptor conformation triggered by this PTH analog, as indicated by experiments with the PTHR conformational biosensor and further elaborated by our computational analysis. We predict that PTH^{7d} likely stabilizes a receptor conformation with a more pronounced outward shift of TM6. It is well established that β-arrestin-GPCR interaction is a two-step binding process (34), whereby the initial β-arrestin interaction with the receptor's phosphorylated C terminus or ICL2/3 is a prerequisite for β-arrestin activation and subsequent engagement to the cytosolic core of a GPCR. Our studies have shown that phosphorylated ICL3 of PTHR is likely a key determinant of initial β-arrestin recruitment to the receptor, whereas the phosphorylated C terminus is required for stabilization of β-arrestin-PTHR complexes. Our computational investigations suggest that PTH^{7d} binding to PTHR may lead to ICL3 positioning closer to the plasma membrane due to a more pronounced outward movement of TM6, potentially rendering ICL3 inaccessible to both phosphorylation and β-arrestin binding. However, we cannot specifically rule out that alanine substitution in ICL3 could confer a conformational change in this region that also precludes the ability to bind β-arrestins. These studies propose a structural basis of β-arrestin recruitment to PTHR that will be experimentally validated in future structural studies.

Previous studies have proposed a paradigm whereby the duration of the cAMP response serves as the major determinant for PTHR-mediated regulation of sCa²⁺ and bone remodeling, and this model has served as the premise for the development of therapeutics targeting the receptor (9, 35, 36). Our findings reveal that a shift in the spatial bias of cAMP signaling from endosomes to the cell surface markedly reduces PTH-induced effects on sCa²⁺ increases and vitamin D activation without altering serum Pi reduction. Our study also raises the prospect that the PTHR-generated endosomal cAMP pool ensures increase in serum vitamin D by inducing the production of the rate-limiting hydroxylase catalyzing the formation of active vitamin D, which subsequently enhances the increase in sCa²⁺. We propose that the PTHR-generated plasma membrane cAMP pool triggers limited nuclear PKA activity and vitamin D increases but might contribute to the inhibition of phosphate transport (Fig. 6). Understanding the mechanism by which endosome-generated cAMP leads to nuclear PKA activity, whereas plasma membrane-generated cAMP does not, will require further studies involving, for example, the importance of cAMP diffusion in cells

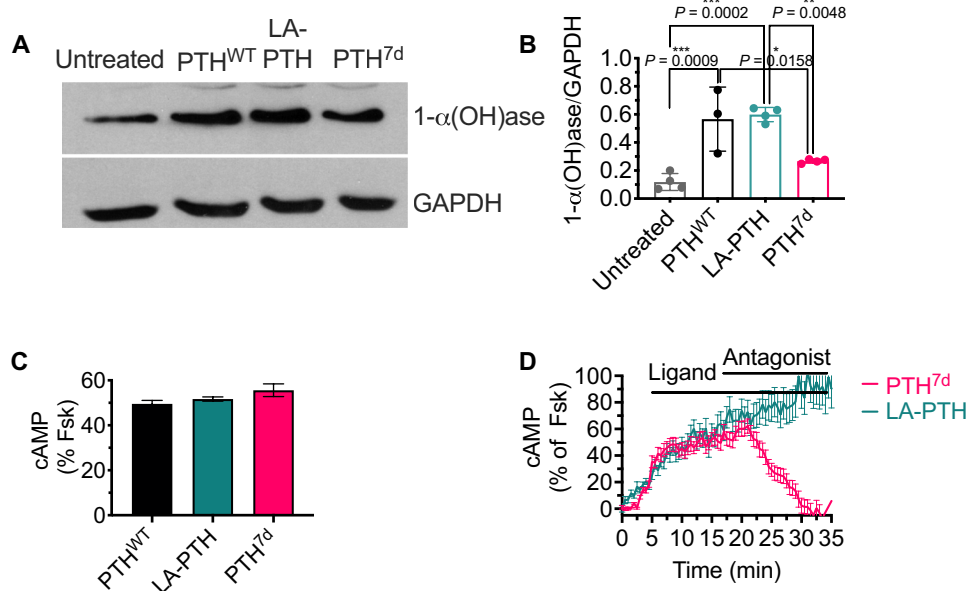


Fig. 5. Basolateral actions of PTH and its variants in polarized MDCK cells. (A and B) Representative Western blot (A) and quantification (B) of 1- α (OH)ase relative to GAPDH in polarized PTHR-expressing MDCK cells after basolateral stimulation with either LA-PTH, PTH^{WT}, or PTH^{7d} for 8 hours. Graph shows individual data points and means \pm SD. P values were determined by one-way ANOVA with Tukey test. The P value for untreated versus PTH^{7d} is 0.25. (C) Quantification of cAMP responses in polarized MDCK cells expressing the Green cADDIs sensor at $t = 30$ min after basolateral stimulation with 100 nM PTH^{WT}, LA-PTH, or PTH^{7d}. Percentage of cAMP responses is relative to the response in the presence of forskolin (Fsk). Data are means \pm SD from $n = 90$ to 107 cells. (D) cAMP time courses in polarized MDCK cells after addition of 100 nM LA-PTH or PTH^{7d} in the absence or presence of 1 μ M d-Trp¹²,Tyr³⁴-bPTH₇₋₃₄, a cell-impermeable competitive antagonist at the basolateral membrane. Horizontal bars indicate the application of ligand and antagonist. Data are means \pm SEM from $n = 48$ cells.

and the role of microdomains in local buffering of cAMP production (37). In addition to the PTHR, several other GPCRs have been reported to engage in cAMP signaling from intracellular compartments, including the vasopressin type 2 receptor (V₂R) (38), glucagon-like peptide 1 receptor (GLP-1R) (39), and the β_1 -adrenergic receptor (β_1 AR) (40) among others, each of which hold potential biological and clinical significance: The V₂R is a major regulator of water homeostasis that acts in the kidneys and has been implicated in nephrogenic diabetes insipidus and heart failure (41); the GLP-1R is well-known to modulate insulin secretion from the pancreas and currently serves as a therapeutic target for the treatment of type 2 diabetes (42); and the β_1 AR contributes to a wide variety of physiological processes, including cardiac function and blood pressure, and currently represents a main therapeutic target for the treatment of hypertension and heart failure (43). This study thus presents implications for other GPCRs that may aid a better understanding of human physiology and facilitate rational drug design in the future.

MATERIALS AND METHODS

Cell culture and transfection

Cell culture reagents were obtained from Corning (Cellgro). HEK cells (HEK293; American Type Culture Collection, Georgetown, DC) stably expressing the recombinant human PTHR were grown in selection medium [Dulbecco's modified Eagle's medium (DMEM), 5% fetal bovine serum (FBS), 5% penicillin/streptomycin, and neomycin (500 μ g/ml)] at 37°C in a humidified atmosphere containing

5% CO₂. For transient expression, cells were seeded on glass coverslips coated with poly-D-lysine in six-well plates and cultured for 24 hours before transfection with the appropriate cDNAs using FuGENE 6 (Promega) or Lipofectamine 3000 (Life Technologies) for 48 to 72 hours before experiments. We optimized expression conditions to ensure that the expression of fluorescently labeled proteins was similar in examined cells by performing experiments in cells displaying comparable fluorescence levels. MDCK cells stably expressing recombinant hemagglutinin (HA)-tagged human PTHR were grown in DMEM/F12 (1:1) supplemented with 5% FBS and 1% penicillin/streptomycin at 37°C in a humidified atmosphere containing 5% CO₂. For polarization of epithelial monolayers, 9.5 \times 10⁴ cells were plated on 24-mm Transwells (Corning) with 0.4- μ m pore size. Cells were used 5 days later, when they reached a transepithelial electric resistance (TER) larger than 500 ohm/cm². TER was measured using an EndOhm-24 SNAP chamber with EVOM resistance meter (World Precision Instruments Inc.) following the manufacturer's instructions.

Chemicals

Forskolin (EMD Millipore, 344270) was used.

Peptide synthesis, purification, and quantification

PTH₁₋₃₄, PTH₁₋₃₄^R, and LA-PTH were synthesized and characterized as previously described (35, 44). (D)-Leu(7)-PTH₁₋₃₄-NH₂ was synthesized by microwave-assisted reactions on NovaPEG Rink amide resin. For each coupling step, the resin was treated with four equivalents of protected amino acid, four equivalents of hexafluorophosphate azabenzotriazole tetramethyl uronium (HATU), and eight equivalents of N,N-diisopropylethylamine in N,N'-dimethylformamide (DMF). 9-Fluorenyl methoxycarbonyl deprotection was carried out by using 20% (v/v) piperidine with 0.1 M hydroxybenzotriazole in DMF. Upon completion of the synthesis, the peptide was cleaved from the resin using a solution of 94% trifluoroacetic acid, 2.5% H₂O, 2.5% 1,2-ethanedithiol, and 1% triisopropylsilane. After the cleavage, the crude peptide was precipitated by addition of cold diethyl ether. The precipitated material was purified by preparative high-performance LC. Peptide purity was assessed by ultrahigh-performance LC (UPLC) [ethylene bridged hybrid (BEH) C18 stationary phase; 2.1 mm by 100 mm; the solvent gradient was 10 to 60% acetonitrile over 5 min], and peptide mass was checked by matrix-assisted laser desorption/ionization-time-of-flight MS. The peptide reported here was >95% pure as determined by UPLC. Because (D)-Leu(7)-PTH₁₋₃₄-NH₂ contains one tryptophan in its sequence, the peptide concentration was determined by ultraviolet (UV) spectroscopy using the absorbance at 280 nm (the molecular extinction coefficient of tryptophan at

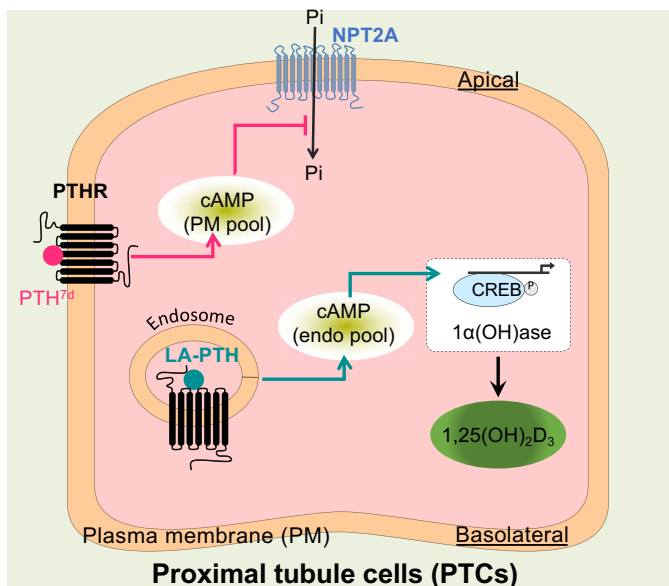


Fig. 6. Proposed model for location bias in cAMP and PTHR pharmacology.

Upon basolateral stimulation of proximal tubule kidney cells, the PTHR-generated endosomal cAMP pool ensures increases in serum vitamin D by inducing the expression of 1- α (OH)ase, the rate-limiting hydroxylase catalyzing the formation of active vitamin D, which subsequently stimulates an increase in sCa^{2+} . The PTHR-generated plasma membrane cAMP pool might contribute to the inhibition of phosphate import, presumably by increasing endocytosis of the Na^+ -dependent phosphate cotransporter 2A (NPT2A). CREB, cAMP response element-binding protein. PM, plasma membrane.

280 nm is $5690 \text{ M}^{-1} \text{ cm}^{-1}$). After concentration determination, the peptide was aliquoted, lyophilized to dry powder, and stored at -20°C . (D)-Ile(5)-PTH₁₋₃₄ (PTH^{5d}), (D)-Gln(6)-PTH₁₋₃₄ (PTH^{6d}), (D)-His(9)-PTH₁₋₃₄ (PTH^{9d}), and (D)-Asn(10)-PTH₁₋₃₄ (PTH^{10d}) were synthesized by LifeTein (catalog numbers 829095, 792338, 756617, and 829096, respectively). The purity of peptides reported by the manufacturer was <98%. Lyophilized peptides were resuspended in 10 mM acetic acid before use.

Plasmids

β -Arr2^{YFP} and PTHR^{SEP} were previously described by the Vilardaga lab (5, 21). β -Arr1^{Rluc8} was provided by Z. Freyberg. G β ₁^{BiFc} [Cer(1-158)-G β ₁] and G γ ₂^{BiFc} [CFP(159-238)-G γ ₂] were a gift from C. Berlot and can be found in Addgene (55707).

Time course measurements of cAMP and β -arrestin recruitment by FRET

Cells were transiently transfected with the FRET-based biosensor, Epac1^{CFP/YFP}, for measuring cAMP or PTHR^{CFP} and β -arr2^{YFP} for measuring arrestin recruitment. Cells plated on poly-D-lysine-coated glass coverslips were mounted in Attofluor cell chambers (Life Technologies); maintained in Hepes buffer containing 150 mM NaCl, 20 mM Hepes, 2.5 mM KCl, and 1 mM CaCl₂, as well as 0.1% bovine serum albumin (BSA) (pH 7.4); and transferred on an inverted Nikon Ti-E equipped with an oil immersion 40 \times numerical aperture (NA) 1.30 Plan Apo objective and a moving stage (Nikon Corporation). Recordings were performed at 37°C using Nikon A1 confocal unit, through a 60 \times NA 1.45 objective (Nikon). Fluorescent proteins containing CFP or YFP were excited with 440- and 514-nm lasers (Melles Griot), respectively. Fluorescence data were

extracted from single cell using Nikon Element Software (Nikon Corporation). The FRET ratio for single cells was calculated and corrected as previously described (45). Individual cells were perfused with buffer or with the ligand for the time indicated by the horizontal bar.

cAMP recordings reported in fig. S4 were performed at room temperature on an inverted Nikon Ti-E epifluorescent microscope to allow visualization of red fluorescent protein-tagged DynK44A. CFP and YFP were excited using a mercury lamp. Fluorescence emissions were filtered using a 480 ± 20 nm (CFP) and 535 ± 15 nm (YFP) of filter set and collected simultaneously with a LUCAS electron multiplying charge-coupled device camera (Andor Technology) using a DualView 2 (Photometrics) with a beam splitter dichroic long pass of 505 nm.

cAMP production in polarized HA-PTHR expressing MDCK cells was measured as follows: Cells were seeded onto inverted 12-mm Transwells (Corning) with a 0.4- μm pore, as previously described (46). After 5 hours of incubation, Transwells were reinverted with the basolateral membrane facing the bottom of a 12-well plate. Cells were cultured for 5 days until polarization was achieved and measured using TER. Two days before imaging, cells were transduced with BacMam containing a Green down cADDIs sensor (Montana Molecular) following the manufacturer's protocol. Transwells were then transferred to an Attofluor cell chamber (Life Technologies) with a glass coverslip at the bottom. Polarized cells, with the basolateral membrane facing the glass coverslip, were imaged on an inverted Nikon Ti-E microscope (confocal Nikon A1) equipped with a Z-driven piezo motor and heated stage. Confocal imaging was performed as described above. The Green down cADDIs sensor was excited with a 488-nm laser. Cells were stimulated with 100 nM ligand, and images were collected every 30 s for 40 min. For antagonist assays, the cell-impermeant PTHR antagonist D-Trp¹², Tyr³⁴-bPTH₇₋₃₄ was added 15 min after ligand stimulation at a final concentration of 1 μM . cAMP signals were calculated as $(\Delta F/F_0)$, corrected for bleaching effect, normalized to the forskolin response, and depicted as the inverse signal because fluorescence intensity of Green cADDIs sensor decreases when the cAMP level increases. Data acquisition and image analysis were done using NIS-Elements Software (Nikon Corporation).

cAMP accumulation assay

HEK293 cells stably expressing the GloSensor cAMP reporter and human PTHR were cultured in DMEM supplemented with 10% FBS. Cells were seeded into 96-well Corning plates and used for cAMP assays after forming a confluent monolayer. Upon the removal of the culture medium, the intact cells in 96-well plates were incubated in CO₂-independent medium containing D-luciferin (0.5 mM) for 20 min at room temperature. After this period, cells in each well were treated with peptides at various concentrations, and luminescence resulting from cAMP production was measured for 30 min on a BioTek Synergy 2 plate reader. The peak luminescence signaling, which usually appeared 14 to 20 min after peptide addition, was used to generate concentration-response curves. The concentration-response curves were fit to the data by using the sigmoidal dose-response equation in Prism 6.0. Reported EC₅₀ and E_{max} values represent means \pm SEM from $N \geq 3$ independent experiments.

Washout assay

For the washout experiments, cells preloaded with D-luciferin were treated with medium (vehicle) or agonists at the concentration of 1 nM for 14 min. After this period, the medium in each well was

removed, and the cells were rinsed twice with CO_2 -independent medium to remove unbound ligand. After the addition of D-luciferin-containing fresh medium to each well, the luminescence was recorded for an additional 150 min. For competitive antagonist-modified wash-out assays, the experimental protocol was as described above except that 0.5 μM of the competitive antagonist [D -Trp¹²,Tyr³⁴]bPTH₇₋₃₄-NH₂ (20) was introduced during the ligand-off phase.

β -Arrestin recruitment by BRET

CHO-FlpIn cells transfected with PTHR^{Fluc8} and β -arr1^{venus} or β -arr2^{venus} were cultured in DMEM supplemented with 10% FBS and hygromycin-B (0.7 mg/ml). Cells were seeded into 96-well plates at a density of 4×10^4 cells per well and cultured for 24 hours before the BRET assay. Cells were rinsed twice with Dulbecco's phosphate-buffered saline (DPBS) to remove traces of phenol red and incubated in fresh DPBS containing coelenterazine-h (at a final concentration of 5 μM) at 37°C for 10 min. After this period, cells in each well were treated with peptides at various concentrations, and BRET readings were collected for 25 min on a BioTek Synergy 2 plate reader with 460/40 and 528/20 nm emission filters. The BRET signal was calculated by subtracting the ratio of 528/20 emission over 460/40 emission for vehicle-treated cells from the same ratio for ligand-treated cells. The peak BRET signals (which usually appeared within the initial 5 min after the peptide addition) were used to generate concentration-response curves. The concentration-response curves were fit to the data by using the sigmoidal dose-response equation in Prism 6.0. Reported EC₅₀ and E_{max} values represent means \pm SEM from $N \geq 3$ independent experiments.

Coimmunoprecipitation

HEK293 cells stably expressing HA-tagged PTHR and cultured on a 10-cm dish were stimulated with PTH^{WT}, LA-PTH, or PTH^{7d} at 100 nM for 5 min. Cells were then washed with ice-cold PBS before cross-linking for 2 hours with dithiobis (succinimidyl propionate) DSP (CovaChem, 13301) in PBS at 4°C. The reaction was stopped by addition of 10 mM tris-HCl for 10 min, and cell lysates were prepared using lysis buffer [1% Triton X-100, 50 mM tris-HCl (pH 7.4), 140 mM NaCl, and 0.5 mM EDTA] containing protease and phosphatase inhibitors (Roche, 11873580001). Protein concentration was determined using a BCA protein assay kit (Thermo Fisher Scientific, 23225), and lysates were incubated with anti-HA agarose antibody beads (Sigma-Aldrich, #A2095, clone HA-7) overnight at 4°C. Elution was done using lithium dodecyl sulfate (LDS) loading buffer (Life Technologies), and samples were loaded on 10% SDS-polyacrylamide gel electrophoresis (PAGE) and transferred to the nitrocellulose membrane. We used antibodies against HA (Covance, clone 16B12) and β -arr1/2 (Cell Signaling, 4674, clone D24H9). Immunoreactive bands were visualized with Luminata Forte (EMD Millipore) and an autoradiography film.

Competition binding at equilibrium in intact live cells

HEK293 cells were stably expressing HA-PTH and were seeded in 96-well plates. After 24 hours, cells were incubated in Hepes buffer [137 mM NaCl/5 mM KCl/1 mM MgCl₂/20 mM Hepes/0.1% BSA (pH 7.4)] for 1 hour at 4°C, followed by 2 hours of incubation at 4°C in the presence of increasing concentrations of unlabeled PTH or PTH^{7d} with a constant PTH^R concentration (31.6 nM). Cells were washed twice with the same buffer, and fluorescence intensities were recorded at 580 \pm 20 nm using an excitation wavelength of

525 \pm 20 nm on a Tecan Spark 20M multimode microplate reader. Nonspecific binding was determined using 1 μM unlabeled ligand. Data were subsequently analyzed using Graphpad Prism 8.0 (GraphPad Software Inc., La Jolla, CA).

Radioligand binding to the R⁰ and R^G PTHR conformations

Ligand binding to the PTHR in the G protein-coupled and G protein-uncoupled conformation, R^G and R⁰, respectively, was assessed by competition methods using membranes prepared from HEK293-G_s-null cells (clone CL2) (47) stably transfected with the PTHR. For membranes used in R^G reactions, the cells were further transfected transiently with a high-affinity G_s-negative dominant (G_s-ND) mutant (48). Binding to R⁰ was assessed using ¹²⁵I-PTH₁₋₃₄ as tracer radioligand, and binding to R^G was assessed using ¹²⁵I-M-PTH₁₋₁₅ as radioligand (48). Binding reactions (100 μl) were assembled at room temperature in membrane binding buffer [20 mM Hepes (pH 7.4), 0.1 M NaCl, 3 mM MgSO₄, 20% glycerol, BSA (3 mg/ml)], protease inhibitors (Sigma-Aldrich Inc., P8849) \sim 20,000 cpm of radioligand, varying amounts of unlabeled ligand and were initiated by addition of cell membranes to a membrane protein concentration of 50 ng/ μl . Reactions were incubated for 90 min at room temperature in 96-well vacuum filtration plates (0.2 μm HPB filter, Millipore Corp.) and terminated by rapid vacuum filtration followed by rinsing with 200 μl of buffer, after which the filters were removed and counted for gamma irradiation. Values of nonspecific binding, maximum binding, and the 50% inhibition constant (IC₅₀) were determined by curve fitting the data using Graphpad Prism 8.0 (GraphPad Software Inc., La Jolla, CA) to a sigmoidal dose-response model with variable slope.

Receptor internalization and recycling

Live imaging trafficking of PTHR^{SEP} was done as described (21) using a Nikon A1 confocal microscope. Briefly, HEK293 cells stably expressing a pH-sensitive GFP variant, superecliptic pHluorin, inserted in the N-terminal domain of the human PTHR^{SEP} were seeded on glass coverslips coated with poly-D-lysine (Sigma-Aldrich, P6407) for 24 hours. Experiments were carried out at 37°C in Hepes buffer used for cAMP experiments. Cells were stimulated by 100 nM ligand for 1 min and then washed out to allow recycling. Images were acquired every 30 s.

ANM analysis

ANM data and methods were originally presented in Clark *et al.* (15). Briefly, we generated a model of PTH-bound receptor using the 3.0-Å cryo-EM structure of active PTHR-G_s complex (PDB 6NBF) (14). This model was inserted into a membrane model consisting of an Simple Cubic (SC) lattice using the Orientations of Proteins in Membranes (OPM) database (49). In the ANM, the protein system (receptor and ligand) is represented as a network where residues (α carbons) serve as the nodes (489 nodes). The membrane accounted for 3953 additional nodes. The overall potential is represented as the sum of harmonic potentials between pairs of nodes within an interaction range (C ^{α} -C ^{α} distance < 15 Å). Normal mode 14 was used for our analysis, and cross-correlations between PTHR Thr³⁹² and PTH residues in this mode are shown in fig. S1. All computations were performed using the ProDy application programming interface (API) (50, 51).

MD system preparation

The 3.0-Å cryo-EM structure of LA-PTH-PTHR-G_s-Nb35 complex (PDB 6NBF) (14) was used to generate initial PTHR models.

Iterative Threading ASSEmby Refinement (I-TASSER) was then used to model flexible loops absent in the cryo-EM structure: extracellular loop (ECD) residues 56 to 104, extracellular loop 1 (ECL1) residues 247 to 275, and ICL3 residues 394 to 398 (52–54). In PyMOL (version 2.1, Schrödinger), structures of G_s, Nb35, palmitic acid, and cholesterol were removed. LA-PTH residues were mutated to the corresponding PTH^{WT} residues, as necessary, using the PyMOL Mutagenesis Wizard. The chirality of Leu⁷ in the PTH^{WT} model was changed in PyMOL to generate the PTH^{7d} model. Each initial model was oriented in a model membrane using the OPM Positioning of Proteins in Membrane (PPM) Server (49). Using oriented models, inputs for Nanoscale Molecular Dynamics (NAMD) were generated using the CHARMM-GUI Membrane Builder (55, 56). Disulfide bonds Cys⁴⁸-Cys¹¹⁷, Cys¹⁰⁸-Cys¹⁴⁸, Cys¹³¹-Cys¹⁷⁰, and Cys²⁸¹-Cys³⁵¹ were specified to ensure correct formation. A heterogeneous lipid bilayer consisting of 75% 1-palmitoyl-2-oleoyl-sn-glycero-3-phosphocholine and 25% cholesterol was assembled around the receptor model using the Replacement Method. The system was solvated in a box of transferable intermolecular potential with 3 points (TIP3P) waters, and ions were added to a concentration of 150 mM NaCl using Monte Carlo sampling.

MD simulations

All-atom simulations were performed in triplicate for PTH^{WT}-PTHR and PTH^{7d}-PTHR simulations using NAMD with the CHARMM36m force field (57, 58). Before production simulations, 10,000 steps of conjugate gradient energy minimization were performed followed by 0.675 ns of equilibration in which restraints were applied and then slowly released over six steps following the protocol established by the CHARMM-GUI group (58). Next, 200 ns of production simulation with 2 fs of time step was performed. Nonbonded interactions were cut off at 12.0 Å, and van der Waals force switching was applied between 10.0 and 12.0 Å. Langevin dynamics and Langevin piston were used to maintain temperature at 303.15 K and pressure at 101.325 kPa.

MD trajectory analysis

MD trajectories were analyzed in Visual Molecular Dynamics (VMD) and PyMOL (59). PTHR snapshots were aligned using receptor TM helices (PTHR^D without ECLs or ICLs: residues 180 to 211, 218 to 246, 280 to 311, 317 to 343, 359 to 392, 399 to 425, and 435 to 460). PTH Glu⁴ hydrogen bond analysis was performed using HBonds Plugin in VMD. The number of hydrogen bonds throughout the trajectories was plotted in GraphPad Prism.

Photocrosslinking in cells

We previously reported a detailed description of this experiment in Clark *et al.* (15). Briefly, we used a β-arrestin mutant with the photo-activatable amino acid *p*-benzoyl-L-phenylalanine incorporated into position 75 of a HA-tagged β-arr1. Photocrosslinking experiments were performed in 10-cm dishes of HEK293 cells expressing a PTHR and the β-arr1 mutant. Twenty-four hours after transfection, cells were stimulated with 200 nM PTH^{WT} or PTH^{7d} for 10 min, washed twice, and irradiated with UV light (365 nm) for 15 min in cold PBS using a UVP cross-linker (Analytik Jena) with 2000× energy exposure (100 μJ/cm²) at a 2.5-cm distance. For coimmunoprecipitation experiments, 150 μl of anti-HA agarose was added to the supernatant and incubated with gentle end-over-end mixing overnight at 4°C. Using centrifugation at 1000g for 5 min at 4°C and aspiration of the supernatant, the beads were washed with radioimmunoprecipitation

assay buffer six times. The protein complex was eluted from the beads by incubating with HA peptide solution (3 mg/ml) for 30 min at 25°C. After centrifugation at 1000g for 5 min at 4°C, the supernatant was collected for subsequent in-gel digestion.

1-α(OH)ase protein expression

MDCK cells stably expressing HA-PTHR were polarized on 24-mm Transwells (Corning) with 0.4-μm pore size. Polarized cells were basolaterally stimulated with 30 nM PTH^{WT}, LA-PTH, or 30 nM PTH^{7D} diluted in growth media, with or without FBS, for 8 hours or left untreated. After stimulation, cells were lysed in lysis buffer containing 50 mM tris (pH 7.4), 150 mM NaCl, 5 mM EDTA, 10% glycerol, and 1% IGEPAL CA-630 (Sigma-Aldrich), supplemented with protease and phosphatase inhibitors, as described before (60). Briefly, Transwells were washed in cold PBS and then membranes were cut out of their plastic supports and put in a microcentrifuge tube with 300 μl of lysis buffer. Membranes were vortexed and incubated in rotation at 4°C for 30 min. Lysates were then centrifuged at maximum speed for 10 min in a benchtop refrigerated centrifuge. Supernatants were transferred to a clean tube. Protein concentration was measured using a BCA protein assay kit (Thermo Fisher Scientific, 23225). For Western blot analysis, 10 μg of lysates was loaded per well of 10% SDS-PAGE. Gels were transferred to a nitrocellulose membrane and blocked in tris-buffered saline with Tween-20 with 5% milk. For detection of 1-α(OH)ase, membranes were blotted with anti-CYP27B1 polyclonal antibody (Novus Biologicals, NBP2-29942) at 1:1000 dilution. Anti-glyceraldehyde phosphate dehydrogenase (GAPDH) monoclonal antibody (Santa Cruz Biotechnologies, sc-32233) at 1:1000 dilution was used as a loading control. Horseradish peroxidase (HRP)-conjugated antibodies (Dako Denmark) were used as secondary antibodies. Immunoreactive bands were visualized with an Immobilon Forte Western HRP substrate (EMD Millipore, WBLUF0100). Band intensity quantification was performed using ImageJ software (National Institutes of Health).

Mouse studies

To test the impact of PTH^{7d}, LA-PTH, and PTH^{WT} (PTH_{1–34}) (Bachem, Torrance, CA; catalog number H-5460) on serum and skeletal parameters, 3-month-old male C57BL/6J (C57/B6) mice (Jackson Laboratory, stock no: 000664) were ear-tagged for identification, randomly assigned to groups, and injected daily with the drugs (40 μg/kg body weight per injection) for 4 weeks after the mice were acclimated with housing environment for 2 weeks. In this study, blood was sampled through the retro-orbital route under isoflurane anesthesia after 2 hours of the last drug injection. The mice were allowed to recover before another blood collection by cardiac puncture and bone collection from the mice euthanized by isoflurane overdose 24 hours after the last drug injection. Serum Ca²⁺ and Pi levels were assessed using an ACE Axcel bioanalyzer (Alfa Wassermann, West Caldwell, NJ), and skeletal parameters of distal femurs were assessed using a SCANCO μCT 50 scanner and analytic software (Scanco USA Inc., Wayne, PA, USA) as detailed previously (61). In a separate time course study, different groups of mice were injected with a single dose of PTH^{WT}, PTH^{7d}, or LA-PTH for different time points before blood collection by cardiac puncture. Their serum 1,25D levels were assessed by an enzyme-linked immunosorbent assay (ELISA) kit (AC-62F1, Immunodiagnostic Systems, Tyne and Wear, UK) according to the manufacturer's instructions. All mice were kept in a climate-controlled room (22°C;

45 to 54% relative humidity) with a 12-hour light/12-hour dark cycle. Water and standard chow (1.3% calcium and 1.03% phosphate) were given ad libitum. All animal experiments (protocol #18-013) were approved and performed according to guidelines of the Institutional Animal Care and Use Committee at the San Francisco Department of Veterans Affairs Medical Center.

Pharmacokinetic analysis

Bioactive LA-PTH or PTH^{7d} content of blood plasma was assessed by applying 5 μ l of plasma (supplemented with protease inhibitors) to the HEK293-derived cell line GP2.3 in which human PTHR and the luciferase-derived GloSensor cAMP reporter were stably expressed. Cells were seeded into 96-well white plates and assayed 24 hours later in CO₂-independent culture medium (Life Technologies, Carlsbad, CA, USA) containing 0.1% BSA. Cells were preincubated with D-luciferin (0.5 mM) for 2 hours, then blood plasma samples were added, and cAMP-dependent luminescence was measured at 2-min intervals. For each well, the maximum luminescence observed, which typically occurred 10 to 20 min after sample addition, was used to establish relative bioactive peptide.

Stable isotope labeling with amino acids in cell culture

We used the HEK293 cell line stably expressing the human HA-tagged PTHR previously generated in our laboratory (62). Three pools of HA-PTHR/HEK293 cells were maintained side by side in SILAC “light,” “medium,” and “heavy” media (fig. S5A). The SILAC media were prepared from custom-ordered DMEM powder without arginine, lysine, and leucine (Gibco, formula no. 03-5080EB) (Gibco/Invitrogen). [²H₄]-L-lysine (50 mg/liter) and [¹³C₆]-L-arginine (25 mg/liter) (Cambridge Isotope Laboratories) were added to the Medium culture medium, and [¹³C₆, ¹⁵N₂]-L-lysine (50 mg/liter) and [¹³C₆, ¹⁵N₄]-L-arginine (25 mg/liter) (Cambridge Isotope Laboratories) were added to the Heavy culture medium, whereas equal concentrations of conventional (i.e., natural) lysine and arginine were added to the Light culture medium. All Light, Medium, and Heavy media were supplemented with L-leucine (104 mg/liter), L-proline (10 mg/liter), 10% dialyzed FBS (Hyclone) (Thermo Fisher Scientific), 1% penicillin/streptomycin, and G418 (150 mg/ml). The SILAC cells were cultured for more than six doublings until the isotope incorporation rates in Medium and Heavy cells were higher than 95%. The SILAC cells were then expanded. When the cells reached ~80% confluence, they were serum-starved for 4 hours. To map the phosphorylation sites on the PTHR induced by PTH^{WT} or PTH^{7d}, the Light-labeled cells cultured in Light medium were treated with 30 nM PTH^{WT} for 5 min before harvesting, the Medium-labeled cells cultured in Medium medium were treated with 30 nM for 5 min before harvesting, and the Heavy-labeled cells cultured in Heavy medium served as control without any treatment. Equal numbers of Light-, Medium-, and Heavy-labeled cells (generally six 150-mm culture dishes each) were mixed, flash-frozen in liquid nitrogen, and stored at -80°C. The SILAC experiments were repeated three times.

HA-PTHR isolation, digestion, and peptide desalting

The HA-PTHRs were isolated from SILAC cells overexpressing HA-PTHR using Pierce Anti-HA Agarose beads (catalog number: 26181, Thermo Fisher Scientific). Briefly, crude membrane fractions were prepared from the equally mixed (Light:Medium:Heavy = 1:1:1) SILAC cells as previously described (27, 63). The HA-PTHRs were

then extracted from crude membrane preparations with 1× buffer [20 mM tris-HCl (pH 8.0), 100 mM NaCl, and 2 mM EDTA] containing 1% DDM (*n*-dodecyl b-D-maltoside), protease inhibitors, and phosphatase inhibitors. HA-PTHRs were isolated from the extraction solution by incubating with 200 μ l of Pierce Anti-HA Agarose beads with rotation at 4°C for 4 hours. The HA-PTHR bound anti-HA Agarose beads were washed with 1× buffer containing 0.1% DDM five times and then eluted with 100 μ l of 2× SDS-PAGE buffer (containing 10 mM dithiothreitol) by incubating at 37°C for 1 hour. The receptor proteins were alkylated with 30 mM iodoacetamide in the dark at room temperature for 30 min. The samples were then subjected to SDS-PAGE separation. The protein bands corresponding to HA-PTHRs were excised from SDS-PAGE gel for in-gel protein digestion.

Tryptic digestion of HA-PTHRs was performed as previously described (64, 65). Briefly, the excised gel bands were chopped into small pieces and destained by distaining solution (50 mM ammonium bicarbonate in 50% acetonitrile). Sequence-grade trypsin (10 ng/ μ l, modified, Promega) in 50 mM NH₄HCO₃ (pH 8.0) was then added to the tubes to cover the destained gel pieces. The tryptic digestion reactions were incubated at 37°C overnight. An equal volume of 100% acetonitrile (CH₃CN) was added to the digested gel samples for peptide extraction and repeated three times. The extracted peptides were pooled into a prewashed protein LoBind tube (catalog number: 13698793, Thermo Fisher Scientific) and then dried under vacuum on a SpeedVac evaporator. The peptide samples were desalting with handmade Stage Tips as previously described (64). The desalting peptides were lyophilized with a SpeedVac evaporator; reconstituted in 0.1% trifluoroacetic acid, 2% acetonitrile, and 25 mM citrate; and subjected to LC-MS/MS analysis.

MS and data analyses

LC-MS/MS analyses were performed on a Thermo Fisher Scientific LTQ Orbitrap Velos mass spectrometer (Thermo Fisher Scientific) with a Finnigan Nanospray II electrospray ionization source. The peptide samples were loaded onto a nanoViper compatible Pico-Chip column (catalog number: 1PCH7515-105H354-NV, New Objective) and separated with a Waters nanoACQUITY UPLC System. Instrument control and primary data processing were done with the Xcalibur software package. The LTQ Orbitrap Velos was operated in a data-dependent mode using a TOP10 strategy (66). MS/MS spectra were searched with the SEQUEST algorithm against a composite database containing the human HA-PTHR sequence or HA-PTHR with its interacting proteins, as well as their reverse sequences. Search parameters allowed for three missed tryptic cleavages, a mass tolerance of \pm 80 parts per million, a static modification of 57.02146 Da (carboxyamidomethylation) on cysteine, and up to eight total dynamic modifications: 79.96633 Da (phosphorylation) on serine, threonine, and tyrosine; 15.99491 Da (oxidation) on methionine; 6.02012 or 10.00827 Da on arginine; and 4.00709 or 8.01420 Da on lysine. Search results were filtered to include <1% matches to reverse sequences by restricting the mass tolerance window and setting thresholds for Xcorr and dCn' (defined as the normalized difference between Xcorr values of the top-ranked candidate peptide and the next candidate with a different amino acid sequence). Matches for phosphopeptides were validated manually with special consideration of intense fragment ions formed through cleavage N terminus to proline residues and neutral losses of phosphoric acid. Peptide quantification was performed with the Vista

program (67) and by manual calculation with the Qual Browser (version 3.0.63). Briefly, the theoretical mass of Light, Medium, and Heavy variants of each peptide was calculated and used to identify ion peaks in the high mass accuracy precursor scans for each. The intensity of the peaks was used to construct ion chromatograms. For each isotopic variant, the peak height and background-subtracted area under the curve were used to calculate the Light-to-Heavy (PTH^{WT}: nonstimulation) and Medium-to-Heavy (PTH^{7d}: nonstimulation) abundance ratios.

Statistics

Data were processed using GraphPad Prism 9.2 and expressed as means \pm SEM or SD. Paired data were statistically compared by using Student's *t* test assuming unequal variances for the two tests. Multiple comparisons were analyzed using one-way or two-way analysis of variance (ANOVA) with Tukey post hoc test.

SUPPLEMENTARY MATERIALS

www.science.org/doi/10.1126/scisignal.abc5944

Figs. S1 to S10

Table S1

[View/request a protocol for this paper from Bio-protocol.](https://bio-protocol.org)

REFERENCES AND NOTES

1. R. Fredriksson, H. B. Schiøth, The repertoire of G-protein-coupled receptors in fully sequenced genomes. *Mol. Pharmacol.* **67**, 1414–1425 (2005).
2. J. Bockaert, J. P. Pin, Molecular tinkering of G protein-coupled receptors: An evolutionary success. *EMBO J.* **18**, 1723–1729 (1999).
3. S. Galandrin, G. Oignly-Longpre, M. Bouvier, The evasive nature of drug efficacy: Implications for drug discovery. *Trends Pharmacol. Sci.* **28**, 423–430 (2007).
4. S. Maudsley, B. Martin, L. M. Luttrell, The origins of diversity and specificity in g protein-coupled receptor signaling. *J. Pharmacol. Exp. Ther.* **314**, 485–494 (2005).
5. S. Ferrandon, T. N. Feinstein, M. Castro, B. Wang, R. Bouley, J. T. Potts, T. J. Gardella, J. P. Vilardaga, Sustained cyclic AMP production by parathyroid hormone receptor endocytosis. *Nat. Chem. Biol.* **5**, 734–742 (2009).
6. D. Calebiro, V. O. Nikolaev, M. C. Gagliani, T. de Filippis, C. Dees, C. Tacchetti, L. Persani, M. J. Lohse, Persistent cAMP-signals triggered by internalized G-protein-coupled receptors. *PLOS Biol.* **7**, e1000172 (2009).
7. I. Sutkeviciute, J. P. Vilardaga, Structural insights into emergent signaling modes of G protein-coupled receptors. *J. Biol. Chem.* **295**, 11626–11642 (2020).
8. T. Dean, J. P. Vilardaga, J. T. Potts Jr., T. J. Gardella, Altered selectivity of parathyroid hormone (PTH) and PTH-related protein (PTHrP) for distinct conformations of the PTH/PTHrP receptor. *Mol. Endocrinol.* **22**, 156–166 (2008).
9. M. Okazaki, S. Ferrandon, J. P. Vilardaga, M. L. Bouxsein, J. T. Potts, T. J. Gardella, Prolonged signaling at the parathyroid hormone receptor by peptide ligands targeted to a specific receptor conformation. *Proc. Natl. Acad. Sci. U.S.A.* **105**, 16525–16530 (2008).
10. V. L. Wehbi, H. P. Stevenson, T. N. Feinstein, G. Calero, G. Romero, J. P. Vilardaga, Noncanonical GPCR signaling arising from a PTH receptor–arrestin–G β complex. *Proc. Natl. Acad. Sci. U.S.A.* **110**, 1530–1535 (2013).
11. T. N. Feinstein, V. L. Wehbi, J. A. Ardura, D. S. Wheeler, S. Ferrandon, T. J. Gardella, J. P. Vilardaga, Retromer terminates the generation of cAMP by internalized PTH receptors. *Nat. Chem. Biol.* **7**, 278–284 (2011).
12. I. Sutkeviciute, L. J. Clark, A. D. White, T. J. Gardella, J. P. Vilardaga, PTH/PTHrP receptor signaling, allostery, and structures. *Trends Endocrinol. Metab.* **30**, 860–874 (2019).
13. M. J. Horwitz, M. B. Tedesco, S. M. Sereika, M. A. Syed, A. Garcia-Ocaña, A. Bisello, B. W. Hollis, C. J. Rosen, J. J. Wysolmerski, P. Dann, C. Gundberg, A. F. Stewart, Continuous PTH and PTHrP infusion causes suppression of bone formation and discordant effects on 1,25(OH)₂ vitamin D. *J. Bone Miner. Res.* **20**, 1792–1803 (2005).
14. L. H. Zhao, S. Ma, I. Sutkeviciute, D. D. Shen, X. E. Zhou, P. W. de Waal, C. Y. Li, Y. Kang, L. J. Clark, F. G. Jean-Alphonse, A. D. White, D. Yang, A. Dai, X. Cai, J. Chen, C. Li, Y. Jiang, T. Watanabe, T. J. Gardella, K. Melcher, M. W. Wang, J. P. Vilardaga, H. E. Xu, Y. Zhang, Structure and dynamics of the active human parathyroid hormone receptor-1. *Science* **364**, 148–153 (2019).
15. L. J. Clark, J. Krieger, A. D. White, V. Bondarenko, S. Lei, F. Fang, J. Y. Lee, P. Doruker, T. Böttke, F. Jean-Alphonse, P. Tang, T. J. Gardella, K. Xiao, I. Sutkeviciute, I. Coin, I. Bahar, J. P. Vilardaga, Allosteric interactions in the parathyroid hormone GPCR-arrestin complex formation. *Nat. Chem. Biol.* **16**, 1096–1104 (2020).
16. I. Bahar, T. R. Lezon, A. Bakan, I. H. Shrivastava, Normal mode analysis of biomolecular structures: Functional mechanisms of membrane proteins. *Chem. Rev.* **110**, 1463–1497 (2010).
17. T. J. Gardella, J. P. Vilardaga, International Union of Basic and Clinical Pharmacology. XCIII. The parathyroid hormone receptors—Family B G protein-coupled receptors. *Pharmacol. Rev.* **67**, 310–337 (2015).
18. J. P. Vilardaga, F. G. Jean-Alphonse, T. J. Gardella, Endosomal generation of cAMP in GPCR signaling. *Nat. Chem. Biol.* **10**, 700–706 (2014).
19. T. J. Gardella, H. Juppner, Molecular properties of the PTH/PTHrP receptor. *Trends Endocrinol. Metab.* **12**, 210–217 (2001).
20. M. E. Goldman, R. L. McKee, M. P. Caulfield, J. E. Reagan, J. J. Levy, C. T. Gay, P. A. De Haven, M. Rosenblatt, M. Chorev, A new highly potent parathyroid hormone antagonist: [D-Trp12,Tyr34]bPTH-(7-34)NH₂. *Endocrinology* **123**, 2597–2599 (1988).
21. J. C. McGarvey, K. Xiao, S. L. Bowman, T. Mamonova, Q. Zhang, A. Bisello, W. B. Sneddon, J. A. Ardura, F. Jean-Alphonse, J.-P. Vilardaga, M. A. Putthenveedu, P. A. Friedman, Actin-sorting nexin 27 (SNX27)-retromer complex mediates rapid parathyroid hormone receptor recycling. *J. Biol. Chem.* **291**, 10986–11002 (2016).
22. F. G. Jean-Alphonse, V. L. Wehbi, J. Chen, M. Noda, J. M. Taboas, K. Xiao, J.-P. Vilardaga, β_2 -adrenergic receptor control of endosomal PTH receptor signaling via G β . *Nat. Chem. Biol.* **13**, 259–261 (2017).
23. V. Sample, L. M. DiPilato, J. H. Yang, Q. Ni, J. J. Saucerman, J. Zhang, Regulation of nuclear PKA revealed by spatiotemporal manipulation of cyclic AMP. *Nat. Chem. Biol.* **8**, 375–382 (2012).
24. D. Mayer, F. F. Damberger, M. Samarasimhareddy, M. Feldmueller, Z. Vuckovic, T. Flock, B. Bauer, E. Mutt, F. Zosel, F. H. T. Allain, J. Standfuss, G. F. Schertler, X. Deupi, M. E. Sommer, M. Hurevich, A. Friedler, D. B. Veprinsev, Distinct G protein-coupled receptor phosphorylation motifs modulate arrestin affinity and activation and global conformation. *Nat. Commun.* **10**, 1261 (2019).
25. S. B. Liggett, Phosphorylation barcoding as a mechanism of directing GPCR signaling. *Sci. Signal.* **4**, pe36 (2011).
26. D. P. Staus, L. M. Wingler, M. Choi, B. Pani, A. Manglik, A. C. Kruse, R. J. Lefkowitz, Sortase ligation enables homogeneous GPCR phosphorylation to reveal diversity in β -arrestin coupling. *Proc. Natl. Acad. Sci. U.S.A.* **115**, 3834–3839 (2018).
27. K. N. Nobles, K. Xiao, S. Ahn, A. K. Shukla, C. M. Lam, S. Rajagopal, R. T. Strachan, T.-Y. Huang, E. A. Bressler, M. R. Hara, S. K. Shenoy, S. P. Gygi, R. J. Lefkowitz, Distinct phosphorylation sites on the β_2 -adrenergic receptor establish a barcode that encodes differential functions of β -arrestin. *Sci. Signal.* **4**, ra51 (2011).
28. J. P. Vilardaga, C. Krasel, S. Chauvin, T. Bambino, M. J. Lohse, R. A. Nissenson, Internalization determinants of the parathyroid hormone receptor differentially regulate β -Arrestin/Receptor association. *J. Biol. Chem.* **277**, 8121–8129 (2002).
29. J. P. Vilardaga, T. J. Gardella, V. L. Wehbi, T. N. Feinstein, Non-canonical signaling of the PTH receptor. *Trends Pharmacol. Sci.* **33**, 423–431 (2012).
30. J. P. Vilardaga, M. Bunemann, C. Krasel, M. Castro, M. J. Lohse, Measurement of the millisecond activation switch of G protein-coupled receptors in living cells. *Nat. Biotechnol.* **21**, 807–812 (2003).
31. D. Wootten, J. Simms, L. J. Miller, A. Christopoulos, P. M. Sexton, Polar transmembrane interactions drive formation of ligand-specific and signal pathway-biased family B G protein-coupled receptor conformations. *Proc. Natl. Acad. Sci. U.S.A.* **110**, 5211–5216 (2013).
32. B. Wang, C. K. Means, Y. Yang, T. Mamonova, A. Bisello, D. L. Altschuler, J. D. Scott, P. A. Friedman, Ezrin-anchored protein kinase A coordinates phosphorylation-dependent disassembly of a NHERF1 ternary complex to regulate hormone-sensitive phosphate transport. *J. Biol. Chem.* **287**, 24148–24163 (2012).
33. H. L. Brenza, C. Kimmel-Jehan, F. Jehan, T. Shinki, S. Wakino, H. Anazawa, T. Suda, H. F. DeLuca, Parathyroid hormone activation of the 25-hydroxyvitamin D3-1alpha-hydroxylase gene promoter. *Proc. Natl. Acad. Sci. U.S.A.* **95**, 1387–1391 (1998).
34. P. Scheerer, M. E. Sommer, Structural mechanism of arrestin activation. *Curr. Opin. Struct. Biol.* **45**, 160–169 (2017).
35. M. Shimizu, E. Joyashiki, H. Noda, T. Watanabe, M. Okazaki, M. Nagayasu, K. Adachi, T. Tamura, J. T. Potts Jr., T. J. Gardella, Y. Kawabe, Pharmacodynamic actions of a long-acting PTH analog (LA-PTH) in thyroparathyroidectomized (TPTX) rats and normal monkeys. *J. Bone Miner. Res.* **31**, 1405–1412 (2016).
36. H. Noda, M. Okazaki, E. Joyashiki, T. Tamura, Y. Kawabe, A. Khatri, H. Jueppner, J. T. Potts Jr., T. J. Gardella, M. Shimizu, Optimization of PTH/PTHrP hybrid peptides to derive a long-acting PTH analog (LA-PTH). *JBMR Plus* **4**, e10367 (2020).
37. A. Bock, P. Annibale, C. Konrad, A. Hannawacker, S. E. Anton, I. Maiellaro, U. Zabel, S. Sivaramakrishnan, M. Falcke, M. J. Lohse, Optical mapping of cAMP signaling at the nanometer scale. *Cell* **182**, 1519–1530.e17 (2020).
38. T. N. Feinstein, N. Yui, M. J. Webber, V. L. Wehbi, H. P. Stevenson, J. D. King Jr., K. R. Hallows, D. Brown, R. Bouley, J. P. Vilardaga, Noncanonical control of vasopressin receptor type 2 signaling by retromer and arrestin. *J. Biol. Chem.* **288**, 27849–27860 (2013).

39. R. S. Kuna, S. B. Girada, S. Asalla, J. Vallentyne, S. Maddika, J. T. Patterson, D. L. Smiley, R. D. DiMarchi, P. Mitra, Glucagon-like peptide-1 receptor-mediated endosomal cAMP generation promotes glucose-stimulated insulin secretion in pancreatic β -cells. *Am. J. Physiol. Endocrinol. Metab.* **305**, E161–E170 (2013).

40. R. Irannejad, V. Pessino, D. Mika, B. Huang, P. B. Wedegaertner, M. Conti, M. von Zastrow, Functional selectivity of GPCR-directed drug action through location bias. *Nat. Chem. Biol.* **13**, 799–806 (2017).

41. M. Boone, P. M. Deen, Physiology and pathophysiology of the vasopressin-regulated renal water reabsorption. *Pflugers Arch.* **456**, 1005–1024 (2008).

42. P. E. MacDonald, W. El-kholby, M. J. Riedel, A. M. F. Salapatek, P. E. Light, M. B. Wheeler, The multiple actions of GLP-1 on the process of glucose-stimulated insulin secretion. *Diabetes* **51** (Suppl 3), S434–S442 (2002).

43. A. Lymeropoulos, G. Rengo, W. J. Koch, Adrenergic nervous system in heart failure: Pathophysiology and therapy. *Circ. Res.* **113**, 739–753 (2013).

44. A. Gidon, M. M. al-Bataineh, F. G. Jean-Alphonse, H. P. Stevenson, T. Watanabe, C. Louet, A. Khatri, G. Calero, N. M. Pastor-Soler, T. J. Gardella, J. P. Vilardaga, Endosomal GPCR signaling turned off by negative feedback actions of PKA and v-ATPase. *Nat. Chem. Biol.* **10**, 707–709 (2014).

45. A. Gidon, T. N. Feinstein, K. Xiao, J. P. Vilardaga, Studying the regulation of endosomal cAMP production in GPCR signaling. *Methods Cell Biol.* **132**, 109–126 (2016).

46. Y. Wakabayashi, J. Chua, J. M. Larkin, J. Lippincott-Schwartz, I. M. Arias, Four-dimensional imaging of filter-grown polarized epithelial cells. *Histochem. Cell Biol.* **127**, 463–472 (2007).

47. W. Stallaert, E. T. van der Westhuizen, A. M. Schönegge, B. Plouffe, M. Hogue, V. Lukashova, A. Inoue, S. Ishida, J. Aoki, C. le Gouill, M. Bouvier, Purinergic receptor transactivation by the β 2-adrenergic receptor increases intracellular Ca^{2+} in nonexcitable cells. *Mol. Pharmacol.* **91**, 533–544 (2017).

48. T. Dean, A. Lingart, M. J. Mahon, M. Bastepe, H. Jüppner, J. T. Potts Jr., T. J. Gardella, Mechanisms of ligand binding to the parathyroid hormone (PTH)/PTH-related protein receptor: Selectivity of a modified PTH(1-15) radioligand for GalphaS-coupled receptor conformations. *Mol. Endocrinol.* **20**, 931–943 (2006).

49. M. A. Lomize, I. D. Pogozheva, H. Joo, H. I. Mosberg, A. L. Lomize, OPM database and PPM web server: Resources for positioning of proteins in membranes. *Nucleic Acids Res.* **40**, D370–D376 (2012).

50. A. Bakan, A. Dutta, W. Mao, Y. Liu, C. Chennubhotla, T. R. Lezon, I. Bahar, Evol and ProDy for bridging protein sequence evolution and structural dynamics. *Bioinformatics* **30**, 2681–2683 (2014).

51. A. Bakan, L. M. Meireles, I. Bahar, ProDy: Protein dynamics inferred from theory and experiments. *Bioinformatics* **27**, 1575–1577 (2011).

52. Y. Zhang, I-TASSER server for protein 3D structure prediction. *BMC Bioinformatics* **9**, 40 (2008).

53. J. Yang, R. Yan, A. Roy, D. Xu, J. Poisson, Y. Zhang, The I-TASSER Suite: Protein structure and function prediction. *Nat. Methods* **12**, 7–8 (2015).

54. A. Roy, A. Kucukural, Y. Zhang, I-TASSER: A unified platform for automated protein structure and function prediction. *Nat. Protoc.* **5**, 725–738 (2010).

55. J. Lee, X. Cheng, J. M. Swails, M. S. Yeom, P. K. Eastman, J. A. Lemkul, S. Wei, J. Buckner, J. C. Jeong, Y. Qi, S. Jo, V. S. Pande, D. A. Case, C. L. Brooks III, A. D. MacKerell Jr., J. B. Klauda, W. Im, CHARMM-GUI input generator for NAMD, GROMACS, AMBER, OpenMM, and CHARMM/OpenMM simulations using the CHARMM36 additive force field. *J. Chem. Theory Comput.* **12**, 405–413 (2016).

56. E. L. Wu, X. Cheng, S. Jo, H. Rui, K. C. Song, E. M. Dávila-Contreras, Y. Qi, J. Lee, V. Monje-Galvan, R. M. Venable, J. B. Klauda, W. Im, CHARMM-GUI Membrane Builder toward realistic biological membrane simulations. *J. Comput. Chem.* **35**, 1997–2004 (2014).

57. J. C. Phillips, R. Braun, W. Wang, J. Gumbart, E. Tajkhorshid, E. Villa, C. Chipot, R. D. Skeel, L. Kalé, K. Schulten, Scalable molecular dynamics with NAMD. *J. Comput. Chem.* **26**, 1781–1802 (2005).

58. J. Huang, S. Rauscher, G. Nawrocki, T. Ran, M. Feig, B. L. de Groot, H. Grubmüller, A. D. MacKerell Jr., CHARMM36m: An improved force field for folded and intrinsically disordered proteins. *Nat. Methods* **14**, 71–73 (2017).

59. W. Humphrey, A. Dalke, K. Schulten, VMD: Visual molecular dynamics. *J. Mol. Graph.* **14**, 33–38 (1996).

60. A. Oztan, M. Silvis, O. A. Weisz, N. A. Bradbury, S. C. Hsu, J. R. Goldenring, C. Yeaman, G. Apodaca, Exocyst requirement for endocytic traffic directed toward the apical and basolateral poles of polarized MDCK cells. *Mol. Biol. Cell* **18**, 3978–3992 (2007).

61. J. D. McElderry, G. Zhao, A. Khmaladze, C. G. Wilson, R. T. Franceschi, M. D. Morris, Tracking circadian rhythms of bone mineral deposition in murine calvarial organ cultures. *J. Bone Miner. Res.* **28**, 1846–1854 (2013).

62. A. D. White, F. Fang, F. G. Jean-Alphonse, L. J. Clark, H. J. An, H. Liu, Y. Zhao, S. L. Reynolds, S. Lee, K. Xiao, I. Sutkeviciute, J. P. Vilardaga, Ca^{2+} allosteric in PTH-receptor signaling. *Proc. Natl. Acad. Sci. U.S.A.* **116**, 3294–3299 (2019).

63. K. Xiao, S. K. Shenoy, Beta2-adrenergic receptor lysosomal trafficking is regulated by ubiquitination of lysyl residues in two distinct receptor domains. *J. Biol. Chem.* **286**, 12785–12795 (2011).

64. A. W. Kahsai, S. Rajagopal, J. Sun, K. Xiao, Monitoring protein conformational changes and dynamics using stable-isotope labeling and mass spectrometry. *Nat. Protoc.* **9**, 1301–1319 (2014).

65. K. Xiao, Y. Zhao, M. Choi, H. Liu, A. Blanc, J. Qian, T. J. Cahill III, X. Li, Y. Xiao, L. J. Clark, S. Li, Revealing the architecture of protein complexes by an orthogonal approach combining HDXMS, CXMS, and disulfide trapping. *Nat. Protoc.* **13**, 1403–1428 (2018).

66. W. Haas, B. K. Faherty, S. A. Gerber, J. E. Elias, S. A. Beausoleil, C. E. Bakalarski, X. Li, J. Villén, S. P. Gygi, Optimization and use of peptide mass measurement accuracy in shotgun proteomics. *Mol. Cell. Proteomics* **5**, 1326–1337 (2006).

67. C. E. Bakalarski, J. E. Elias, J. Villén, W. Haas, S. A. Gerber, P. A. Everley, S. P. Gygi, The impact of peptide abundance and dynamic range on stable-isotope-based quantitative proteomic analyses. *J. Proteome Res.* **7**, 4756–4765 (2008).

Acknowledgments: We are grateful to A. Inoue (U. Tohoku) for advice in using G_s -null cells.

Funding: Research reported in this publication was supported by grants from the U.S. National Institutes of Health (NIH) (R01-DK111427 and R01-DK116780 to J.-P.V., R01-DK122259 to J.-P.V. and W.C., R01-AR067291 to W.C., DK11794 and AR066261 to T.J.G., R01-GM-056414 to S.H.G., P41-GM103712 and R01-GM139297 to I.B., and F31-AR074843 to L.J.C.) and the Department of Veterans Affairs (I0-BX003453-03 and IKB6BX004835 to W.C.).

Author contributions: A.D.W., K.A.P., S. Lei, and F.G.J.-A. performed signaling experiments. S. Liu and S.H.G. synthesized PTH⁷⁻¹² and conducted preliminary assessment of the agonism profile that identified the G protein bias of this peptide. T.J.G. performed radioligand binding assays. L.J.C. performed MD simulations. W.C., Z.C., C.S.M., and C.-L.T. performed mouse studies. N.S., C.S.M., and C.-L.T. performed serum chemistry and 1,25D and/or skeletal analyses. J.Y.L. and I.B. performed ANM analysis. F.F. and K.X. performed MS experiments. The authors analyzed and discussed the data. J.-P.V. was responsible for the overall conceptual composition and supervision of the study. A.D.W., L.J.C., K.A.P., W.C., I.S., and J.-P.V. wrote the manuscript.

Competing interests: S.L. and S.H.G. are co-inventors on a patent application that includes PTH⁷⁻¹². S.H.G. is a cofounder of and has a secondary affiliation with Longevity Biotech Inc. The other authors declare that they have no competing interests. **Data and materials availability:** The MS data have been deposited in the ProteomeXchange Consortium with the dataset identifier (MSV000087510/PXD026256). All other data needed to evaluate the conclusions in the paper are present in the paper or in the Supplementary Materials. All materials, data, animal models, and associated protocols will be made available upon reasonable request.

Submitted 3 May 2020

Resubmitted 18 November 2020

Accepted 9 September 2021

Published 5 October 2021

10.1126/scisignal.abc5944

Citation: A. D. White, K. A. Peña, L. J. Clark, C. S. Maria, S. Liu, F. G. Jean-Alphonse, J. Y. Lee, S. Lei, Z. Cheng, C.-L. Tu, F. Fang, N. Szeto, T. J. Gardella, K. Xiao, S. H. Gellman, I. Bahar, I. Sutkeviciute, W. Chang, J.-P. Vilardaga, Spatial bias in cAMP generation determines biological responses to PTH type 1 receptor activation. *Sci. Signal.* **14**, eabc5944 (2021).

Spatial bias in cAMP generation determines biological responses to PTH type 1 receptor activation

Alex D. WhiteKarina A. PeñaLisa J. ClarkChristian Santa MariaShi LiuFrédéric G. Jean-AlphonseJi Young LeeSaifei LeiZhiqiang ChengChia-Ling TuFei FangNicholas SzetoThomas J. GardellaKunhong XiaoSamuel H. GellmanVet Baharleva SutkeviciuteWenhan ChangJean-Pierre Vilardaga

Sci. Signal., 14 (703), eabc5944.

Location matters for GPCR signaling

Parathyroid hormone (PTH) receptor (PTHR) is a G protein-coupled receptor (GPCR) that controls vitamin D, Ca, and bone homeostasis by stimulating cAMP production at the plasma membrane and at endosomes after β -arrestin-dependent internalization. White *et al.* generated a synthetic PTH derivative (PTH) that inhibited β -arrestin coupling to PTHR, thereby leading to sustained cAMP production at the cell surface. Comparison of cellular and organismal responses to wild-type PTH, PTH, or a PTH analog that elicits sustained endosomal signaling demonstrated that the biological outcome was determined by the subcellular location of PTHR activity. These findings suggest that biological responses elicited by other GPCRs that are active at intracellular compartments may show a similar dependence on the location of signaling.

View the article online

<https://www.science.org/doi/10.1126/scisignal.abc5944>

Permissions

<https://www.science.org/help/reprints-and-permissions>